EFFICIENT FREQUENCY-DOUBLING OF FEMTOSECOND PULSES IN WAVEGUIDE AND BULK NONLINEAR CRYSTALS

Design, fabrication, theory and experiment

Ben Agate[1], Edik U. Rafailov[2], Wilson Sibbett[1], Solomon M. Saltiel[3], Kaloian Koynov[4], Mikael Tiihonen[5], Shunhua Wang[5], Fredrik Laurell[5], Philip Battle[6], Tim Fry[6], Tony Roberts[6] and Elizabeth Noonan[6]

[1]School of Physics and Astronomy, University of St Andrews, St Andrews, KY16 9SS, Scotland, U.K.; [2]Division of Electronic Engineering and Physics, University of Dundee, Dundee, DD1 4HN, Scotland, U.K.; [3]Faculty of Physics, University of Sofia, 5 J. Bourchier Boulevard, BG-1164, Sofia, Bulgaria; [4]Max Planck Institute for Polymer Research, Ackermannweg 10, D-55128 Mainz, Germany; [5]Department of Physics, Royal Institute of Technology, Roslagstullsbacken 21, SE-10691 Stockholm, Sweden; [6]AdvR Inc., Suite K, 910 Technology Boulevard, Bozemon, Montana 59718, USA

Abstract: We investigate efficient frequency-doubling of low energy femtosecond pulses in bulk and waveguide nonlinear crystals, thereby demonstrating how to achieve a compact and portable ultrafast blue light source. Using a femtosecond Cr:LiSAF laser (fundamental wavelength 860 nm), we examine the relative merits of the process of second harmonic generation (SHG) using bulk potassium niobate, bulk aperiodically-poled KTP, periodically-poled and aperiodically-poled KTP waveguide crystals. While SHG conversion efficiencies up to 37% were achieved using the waveguides, non-traditional strong focusing in the bulk samples yielded efficiencies of 30%. We have developed several theoretical models to accurately describe the temporal and spectral properties of the generated blue light, as well as the observed saturation behavior of the conversion process in the waveguide structures.

Key words: Diode-pumped lasers; frequency conversion; modelocked lasers; waveguides; periodic structures, quasi-phasematching, femtosecond pulses.

S. Janz et al. (eds.), Frontiers in Planar Lightwave Circuit Technology, 189–227.

1. INTRODUCTION

The recent progress in photobiology research, such as microscopy, optical micromanipulation and bio-medical imaging continues to justify the need for compact, low-cost visible and near-infrared lasers that demonstrate true portability and practicality. The development and exploitation of photonics-based techniques that are applicable to biology and medicine is of particular interest. Laser sources at the shorter blue and ultraviolet wavelengths provide clear advantages over infrared lasers in allowing for stronger beam focusing, enhanced resolution in multi-dimensional imaging techniques[1] and high-resolution spectroscopy[2]. By using ultrashort-pulse lasers in preference to continuous-wave sources, it is possible to investigate ultrafast biological processes[3], increase the resolution of microscopy[4,5], and amplify subtle signals in nonlinear and multi-photon techniques[6-8]. Femtosecond pulses in the blue spectral region have already been utilized in the study of protein dynamics[9].

Straightforward frequency-doubling of near-infrared femtosecond lasers remains one of the simplest and most efficient access routes into the blue spectral region, due mainly to the inherently high peak intensities of the ultrashort laser pulses. While conventional titanium-sapphire lasers have long been the market leader in providing femtosecond pulses in the near-infrared, their impractical size, cost and power requirements render such sources impractical for space-limited on-site applications in bio-medical and clinical laboratories. Consequently, we have recently demonstrated how small-scale femtosecond Cr:LiSAF lasers have much to offer in combining superior operational efficiencies with impressive design flexibility[10].

In this paper, we begin by describing second harmonic generation (SHG) in the femtosecond regime. We then present several theoretical models which accurately describe efficient SHG of femtosecond pulses in both bulk and waveguide nonlinear crystal structures, and detail the design and fabrication processes of these samples. We describe how a compact Cr:LiSAF laser design can be used to demonstrate an attractively simple approach to developing a portable ultrafast blue light source[11]. With this femtosecond Cr:LiSAF laser (operating at around 850 nm), we then experimentally access the blue spectral region with a series of SHG investigations using four types of nonlinear crystal. The performance of aperiodically-poled potassium titanyl phosphate (appKTP) in bulk and waveguide form is assessed in comparison to bulk potassium niobate ($KNbO_3$)[12] and periodically-poled KTP (ppKTP) waveguide[13]. Each nonlinear crystal is placed in a very simple extra-cavity single-pass arrangement at room temperature, requiring minimal wavelength and temperature stabilization. The ultrashort-pulse blue light generated from all

four nonlinear crystals is either femtosecond or picosecond in duration. This investigation provides the means to compare and contrast the relative merits of bulk and waveguide nonlinear materials, as well as periodically- and aperiodically-poled structures. Observations show that, while superior infrared-to-blue SHG efficiencies are achieved with bulk $KNbO_3$ and the ppKTP waveguide, aperiodically-poled structures permit higher blue peak powers, shorter blue pulses and broader tunability in the blue spectral region. To support our experimental findings, we analyze the crystal performances against our mathematical models, before concluding with a discussion and summary.

2. FREQUENCY-DOUBLING OF FEMTOSECOND PULSES

2.1 Background

The theoretical study of second harmonic generation (SHG) using focused Gaussian beams by Boyd and Kleinman[14] has long been a reliable resource for those studying frequency conversion processes. However, the Boyd-Kleinman theory applies only to cw beams, and cannot be relied upon to correctly describe harmonic generation using ultrashort (femtosecond) pulses. We have recently published a theoretical model[15] that describes SHG of femtosecond pulses in bulk nonlinear crystals, by taking into account the associated critical effects of group velocity mismatch (GVM). Our model explains successfully the experimentally observed behavior of SHG in the femtosecond regime[12,16], in contrast to the somewhat inaccurate predictions of Boyd and Kleinman. We have also adapted this model to describe SHG of femtosecond pulses in waveguide nonlinear crystals[11,13], which accurately describes the observed saturation of the SHG conversion process.

The efficiency of any parametric process is subject to limitations imposed by GVM, which describes a temporal walk-off between the interacting beams. This walk-off arises from a mismatch in the group velocities, and becomes particularly significant in the ultrashort pulse regime. Second harmonic generation under conditions of large GVM is characterized by a nonstationary length, L_{nst}, defined by $L_{nst} = \tau/\alpha$, where τ is the time duration of the fundamental pulses, and the GVM parameter, $\alpha = 1/v_2 - 1/v_1$, where v_2 and v_1 are the group velocities of the second harmonic (SH) and fundamental wave respectively. The nonstationary length, L_{nst}, is the distance at which two initially overlapped pulses at different wavelengths become separated by a time equal to τ. In the ultrashort pulse limit (i.e. for $L_{nst} << L$, where L is the length of the nonlinear media) and for the case

of an unfocused fundamental beam, the generated SH pulses are longer in time by a factor L/L_{nst}. In contrast to the well known quadratic dependence for the frequency doubling of cw waves, this process depends linearly on the length of the nonlinear media, L. As a result of this deleterious temporal broadening effect, nonlinear media are often chosen such that $L \approx L_{nst}$. However, while this may ensure generated SH pulses having durations close to that of the fundamental pulses, the interaction length is reduced and the SHG efficiency is compromised.

The natural way to increase the efficiency of such a frequency conversion process is to use a focused fundamental beam (or, alternatively, a waveguide structure). An established theory of SHG using focused cw beams[14] predicts, for negligible birefringence walk-off, an optimal focusing condition which is expressed by the ratio $L/b = 2.83$, where b is the confocal parameter ($b = k_1 w_{01}^2$, where w_{01} and k_1 are the focal spot radius and the wave vector of the fundamental wave respectively). However, this theory applies only to the long-pulse or cw case, where GVM is negligible ($L_{nst} >> L$). Our recently published theoretical model[15] defines, for the first time, the optimum focusing conditions for SHG using focused beams in the ultrashort-pulse regime, where GVM is significant (i.e. where $L \geq L_{nst}$).

Despite the limitations imposed on the length of the nonlinear media by the unwanted effects of GVM, several experimental papers on frequency doubling in $KNbO_3$[12,16-19], LBO[20] and BBO[20] have recently demonstrated that efficient SHG is possible by focusing femtosecond (120-200 fs) pulses in "thick" nonlinear media where the ratio $L/L_{nst} > 20$. These experiments have demonstrated that a conversion efficiency exceeding 60% is possible and, as we have shown[12], the duration of the generated near-transform-limited SH pulses remained within the femtosecond regime, increasing only 2-3 times with respect to the fundamental duration. In these experiments the optimal ratio L/b was found to be in the region of 10, which is far from the known Boyd and Kleinman ratio of $L/b = 2.83$. To our knowledge, no other theoretical investigations exist that can predict the optimal focusing for SHG under conditions of large GVM, as we discuss here. In the reported work of Weiner and Yu[16,19] a simple model is proposed that predicts well the efficiency of the SHG process in bulk nonlinear crystals, as well as identifying that an increase in SHG efficiency relates to an increase in the L/b ratio. Their model, however, does not predict the existence of optimal values for L/b and phase mismatch as obtained in both experiments discussed above. Also, it cannot describe the evolution of the SH temporal shape inside the crystal and does not give an optimal focusing position inside the nonlinear media.

Our theoretical model for SHG in bulk nonlinear crystals, which describes the process of SHG under conditions of large GVM, assumes an

undepleted fundamental beam, and that both the fundamental and SH beam have Gaussian transverse distributions. The results of the model are later compared with experimental data from SHG experiments using focused femtosecond pulses in the bulk nonlinear crystals of potassium niobate ($KNbO_3$) and aperiodically-poled potassium titanyl phosphate (appKTP). This model is presented in section 2.2.

In the case of SHG in waveguide nonlinear crystals, we describe a theoretical model which accounts for the temporal behavior of the interacting pulses and the possible *z*-dependence of the phasematching condition. The model also describes the observed saturation and subsequent decrease in SHG conversion efficiency in the waveguide samples, as a result of two-photon absorption (TPA) of the second harmonic (SH) wave. The results of this model are later compared with experimental data from SHG experiments using femtosecond pulses in the waveguide nonlinear crystals of periodically-poled potassium titanyl phosphate (ppKTP) and appKTP. This model is presented in section 2.3.

2.2 Theoretical model to describe SHG of focused femtosecond pulses in periodically-poled and aperiodically-poled bulk nonlinear crystals

As discussed above, we have recently reported a theoretical model that defines the optimal conditions for SHG using focused beams in the ultrashort-pulse regime. The model[15], verified by experiment[12], is suitable for cases when birefringence walk-off can be neglected, such as SHG with non-critical phasematching (as with $KNbO_3$) and SHG in a homogeneous quasi-phasematched structure[21]. It provides information on the efficiency of the SHG process, the pulse duration of the SH pulses (figure 1a), and the modification of the phasematching tuning curves. It also allows for optimization of the SHG process by selecting the optimal phase mismatch, focusing strength (figure 2) and position of focusing within the crystal.

Here we will show that our previous model[15] can be extended to describe the process of SHG with focused beams in aperiodically-poled nonlinear media (i.e. those with inhomogeneous mismatch).

While inhomogeneous mismatch can result from a non-constant temperature variation along the sample length, we will instead consider the typical case of a $\chi^{(2)}$ crystal with linearly chirped quasi-phasematched (QPM) grating. The crystal is a nonlinear medium with a locally varying phasematching parameter. For a linearly chirped quasi-phasematched (QPM) grating the mismatch phase factor, $\Phi(z)$, which controls the second harmonic generation process at point z can be presented in the form

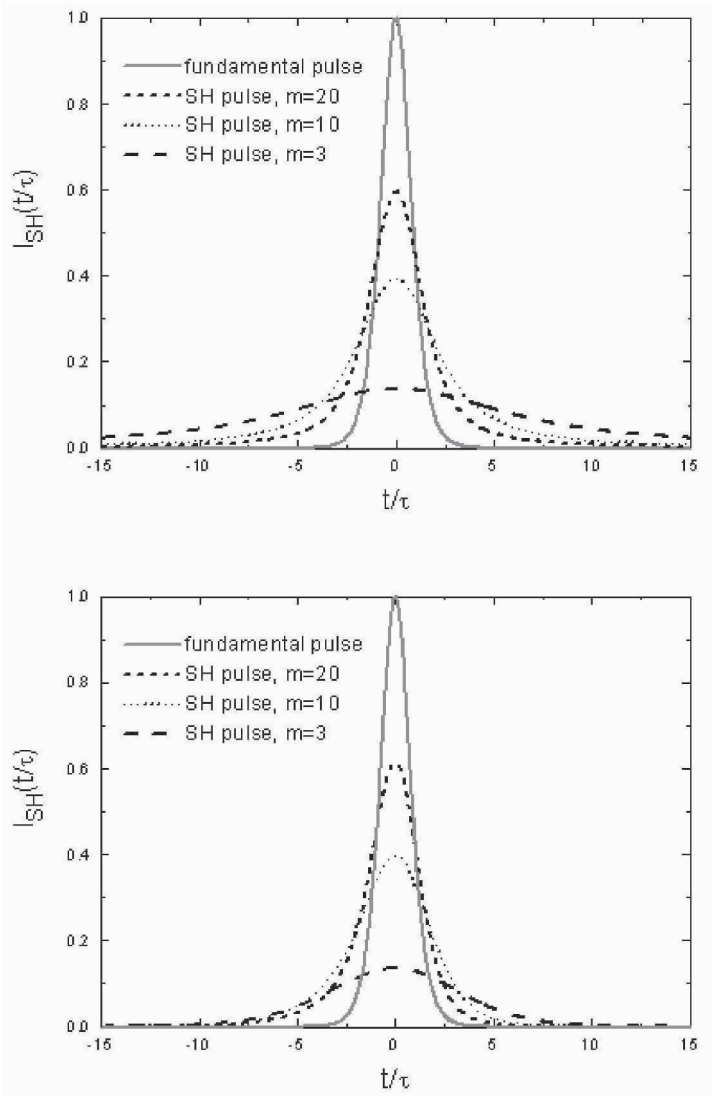

Figure 1. Temporal profiles and relative intensities of the generated SH pulses calculated for several values of focusing strength, $m = L/b$, and ratio $L/L_{nst} = 40$ for: (a) uniform (periodically-poled) nonlinear media[15]; and (b) linearly chirped (aperiodically-poled) quasi-phasematched grating with $\Delta\Lambda = 0.2\ \mu m$ ($D_g = 10.3\ mm^{-2}$). The fundamental pulse shape (grey line) is shown for comparison.

$\Phi(z) = \Delta k_0 z + D_g z^2$, which allows the localized wavevector imbalance to be presented as $\Delta k(z) = d\Phi(z)/dz = \Delta k_0 + 2D_g z$, where D_g is calculated from $D_g = \pi\Delta\Lambda/\left(\Lambda_0^2 L\right)$ and $\Delta k_0 = k_2 - 2k_1 - 2\pi/\Lambda_0$. The quantity $\Delta\Lambda = \Lambda(z = L) - \Lambda(z = 0)$ defines the change of the grating period across the

sample length, L, and $\Lambda_0 = \left[\Lambda(z=L)+\Lambda(z=0)\right]/2$ is the mean grating period. It is useful to note that for sufficiently long samples (as is the case for both $KNbO_3$ and appKTP samples used in our experiments, described in sections 7.1 and 7.2), the variation of the grating period across the sample, $\Delta\Lambda$, defines the wavelength acceptance bandwidth, $\Delta\lambda_{fund}$, of the SHG process in the case of unfocused or weakly focused beams:

$$\Delta\lambda_{fund} = \left|\frac{2\pi\Delta\Lambda}{\Lambda_0^2}\left(\frac{d\Delta k_0}{d\lambda}\right)^{-1}\right| \tag{1}$$

The parabolic equations derived in a slowly varying envelope approximation that describe the second harmonic generation (SHG) of ultrashort pulses in media with locally inhomogeneous wave-vector mismatch, have the form:

$$\left(\frac{\partial}{\partial z}+\frac{i}{2k_1}\Delta_\perp+\frac{1}{v_1}\frac{\partial}{\partial t}\right)A_1 = 0 \tag{2}$$

$$\left(\frac{\partial}{\partial z}+\frac{i}{2k_2}\Delta_\perp+\frac{1}{v_2}\frac{\partial}{\partial t}\right)A_2 = -i\sigma_2 A_1^2\exp(i\Phi(z)) \tag{3}$$

where A_1 and A_2 denote the complex amplitudes of the fundamental and the second harmonic wave respectively, and are functions of three spatial coordinates and one temporal coordinate, $A_j = A_j(x,y,z,t)$. $\Delta_\perp$ stands for the operator $\partial^2/\partial x^2 + \partial^2/\partial y^2$. The nonlinear coupling coefficient, σ_2, is calculated as $\sigma_2 = 2\pi d_{\text{eff, SHG}}/(\lambda_1 n_2)$, where the magnitude of $d_{\text{eff, SHG}}$ depends on the method of phase-matching and the type of the nonlinear medium that is used. The depletion of the fundamental beam, birefringence walk-off and absorption losses for the both interacting waves are neglected.

Following the previously described method[15] we obtain an expression for the SH amplitude, $S(L, p)$, at the output of a nonlinear media with linearly chirped (aperiodically-poled) quasi-phase-matched (QPM) grating:

$$S(L,p) = -i\sigma_2 A_o^2 b H_{tr}(m,\mu,\nu,\gamma,p) \tag{4}$$

with

$$H_{tr}(m,\mu,\nu,\gamma,p)=\frac{1}{2}\int_{-m(1+\mu)}^{m(1-\mu)}\frac{\mathrm{d}u}{1-iu}T\left(\frac{p}{\tau}+\gamma u\right)^2\exp(i\nu u+iD_g b^2u^2/4) \qquad (5)$$

where $\nu=\frac{\Delta k_o b}{2}=\frac{\Delta k_o L}{2m}$; $m=\frac{L}{b}$; $\gamma=\frac{\alpha b}{2\tau}=\frac{1}{2m}\frac{L}{L_{nst}}$ and μ indicates the position of the focused spot inside the crystal: $\mu=0$ corresponds to center of the crystal; $\mu=-1$ to the focus at the input face; $\mu=+1$ to the focus at the output face. In addition, p is the local time, α is the GVM parameter, and τ is related to the full-width at half-maximum (FWHM) fundamental pulse duration, τ_0, by $\tau=\tau_0/1.76$.

The energy of the second harmonic (SH) is found by integrating the SH intensity over space and time while assuming Gaussian spatial and hyperbolic secant temporal profiles. The normalized efficiency, η_0 (%pJ^{-1}), of the SHG process is then calculated by:

$$\eta_o=\frac{16\pi^2d_{eff}^2}{3\lambda^3c\varepsilon_o n_2n_1}\frac{Lh_{tr}}{\tau}10^{-10} \qquad (6)$$

where n_2 and n_1 are respectively the refractive indices at the second harmonic and fundamental wavelengths, and h_{tr} is a transient focusing factor calculated from

$$h_{tr}(m,\mu,\nu,\gamma)=\frac{3}{4m}\int_{-\infty}^{+\infty}\left|H_{tr}(m,\mu,\nu,\gamma,p')\right|^2dp' \qquad (7)$$

The absolute efficiency, η (%), in the absence of depletion of the fundamental wave is defined by $\eta=\eta_0W_{fund}$, where W_{fund} is the fundamental pulse energy in pJ. At higher pump intensities, when the depletion of the fundamental is weak but essential, the corrected value for the absolute efficiency, η (%), can be found by[20]:

$$\eta=\frac{100W_{fund}\eta_o}{100+W_{fund}\eta_o} \qquad (8)$$

By controlling the parameter D_g, defined above as $D_g=\pi\Delta\Lambda/(\Lambda_0^2L)$, we can apply this model to accurately describe the SHG process in linearly chirped (aperiodically-poled) QPM structures with focused beams. $D_g=\Delta\Lambda=0$ corresponds to homogeneous (periodically-poled) QPM

gratings, and for this case the model provides the results described previously[15]. $D_g \neq 0$; $\Delta\Lambda \neq 0$ corresponds to inhomogeneous (aperiodically-poled) QPM structures, and the results of the model in describing the generated SH pulse shape are presented in figure 1b. Figure 2 provides theoretical curves which define the optimal SHG focusing conditions for different values of $\Delta\Lambda$.

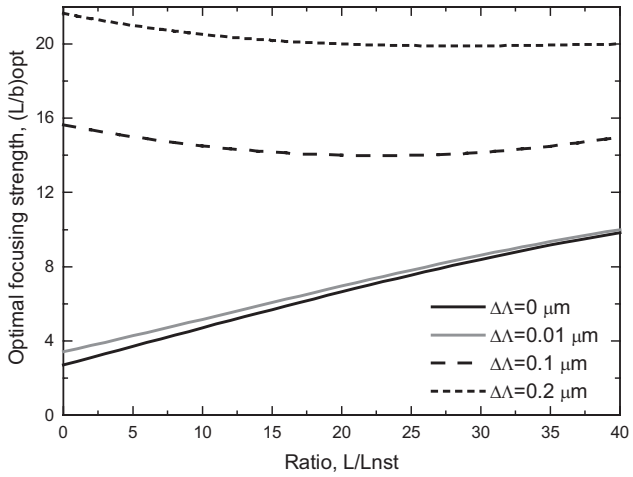

Figure 2. Dependence of optimal focusing strength, $m_{opt} = (L/b)_{opt}$, on the ratio, L/L_{nst} for different values of $\Delta\Lambda$. Crystal length is $L = 4$ mm. The efficiency of the SHG process can be maximized by selecting the correct focusing lens for a given ratio L/L_{nst}.

As can be seen from the comparison of figure 1a and figure 1b, the SH pulse duration is shorter when the SHG process takes place in linearly chirped QPM structures. The output pulses also have certain amount of phase chirp, which can be exploited to achieve further pulse shortening[22,23]. Figure 1 perfectly illustrates the advantage of using relatively thick nonlinear crystals with focused beams: the generated SH intensity is higher and the pulses are shorter in the case of tight focusing (i.e. larger $m = L/b$).

As illustrated in figure 2 the strong dependence of the optimum focusing strength, $m_{opt} = (L/b)_{opt}$, on the ratio L/L_{nst} (which is typical for materials with constant Δk) no longer applies when dealing with aperiodically-poled structures (those with a linear change of Δk in z).

We believe that our model can be extended even further to accurately describe other nonlinear optical interactions such as sum and difference frequency mixing, as well as higher-order harmonics generation.

2.3 Theoretical model to describe SHG of femtosecond pulses in waveguide nonlinear crystals

As mentioned earlier, second harmonic generation using femtosecond pulses is characterized by group velocity mismatch (GVM), which accounts for the temporal walk-off between the fundamental and second harmonic pulses in propagation through the nonlinear medium. The nonstationary length, L_{nst}, introduced earlier and defined by $L_{nst} = \tau/\alpha$ (where τ is the time duration of the fundamental pulses, and $\alpha = 1/v_2 - 1/v_1$) also plays a vital role when considering SHG of femtosecond pulses in waveguide structures. When the sample thickness, $L >> L_{nst}$, the regime is called 'nonstationary' and there are two important consequences: a) the generated SH pulses are L/L_{nst} times longer than the fundamental pulse; and b) in contrast to the well known *quadratic* dependence of the SH efficiency on the length of the nonlinear media, the process of SHG with femtosecond pulses in the nonstationary regime depends *linearly* on the length of the nonlinear media. The reason for this linear dependence reflects the fact that the second harmonic signals generated in each of the different crystal slices with length L_{nst} do not interfere constructively - the energy of the generated SH is simply the sum of the SH energies generated in each slice. This allows us to use a very simple formula to describe the process of SHG in the nonstationary regime ($L >> L_{nst}$), which applies to both SHG in bulk media with unfocused beams, and to SHG in waveguided crystals.

In deriving the formula we require, let us first recall that the amplitude of phasematched SHG in a sample with $L = L_{nst}$ in an undepleted approximation is described by the differential equation:

$$\frac{dA_2}{dz} = -i\sigma_2 A_1 A_1 \tag{9}$$

The solution of Eq. (9) gives for the power of the SH wave:

$$P_2 = \frac{2\sigma_2^2}{\varepsilon_o nc}\frac{P_1^2}{A_{eff}} L_{nst}^2 \tag{10}$$

where P_1 is the power of the fundamental wave, and A_{eff} is the effective cross section of the waveguide. Rewriting this expression in terms of energy we obtain an expression for the SHG efficiency:

$$\eta = \frac{W_2}{W_{fund}} = \frac{2\sigma_2^2}{\varepsilon_o nc} \frac{W_{fund}}{A_{eff}\tau} L_{nst}^2 \tag{11}$$

where W_2 and W_{fund} are respectively the SH and fundamental pulse energies. If now the waveguide length is several times longer than L_{nst}, then the output energy is scaled by the factor L / L_{nst}:

$$\eta_{nd} = \frac{2\sigma_2^2}{\varepsilon_o nc} \frac{W_{fund} L_{nst}^2}{A_{eff}\tau} \frac{L}{L_{nst}} = \frac{8\pi^2 \left| d_{eff}^{(2)} \right|^2}{\varepsilon_o c n^3 \lambda^2} \frac{W_{fund} L}{\alpha A_{eff}} \tag{12}$$

For bulk samples the effective cross-section, $A_{eff} = \pi w_{01}^2$. It can be seen from Eq. (12) that SHG energy conversion in the nonstationary regime ($L >> L_{nst}$) depends linearly on the length of nonlinear media and does not depend on the pulse duration. Equation (12) can be recovered from the results of Weiner[16] if we take weak focusing approximation of their Eq. (4).

We remind the reader that Eq. (12) is derived under conditions where the effects of pump depletion are neglected. In much the same way as it was described in section 2.2, we can expand the application of Eq. (12) for the range of higher pump intensities for which the depletion of the fundamental is weak but essential. The corrected value for the SHG efficiency, η_{cor}, which accounts for the effects of pump depletion is[20]:

$$\eta_{cor} = \frac{\eta_{nd}}{1 + \eta_{nd}} \tag{13}$$

We will later use Eq. (13) for analyzing the experiments of SHG in ppKTP and appKTP waveguides (described in section 7). For now, we compare the analytical solution of Eq. (13) with the direct numerical solution of the differential equations in Eq. (14), which account for the temporal behavior of the interacting pulses, the nonlinear losses of the SH wave, and the possible *z*-dependence of the phasematching condition:

$$\left(\frac{\partial}{\partial z}+\frac{1}{v_1}\frac{\partial}{\partial t}\right)A_1 = -i\sigma_1 A_2 A_1^* \exp\left[-i\Phi(z)\right]$$
$$\left(\frac{\partial}{\partial z}+\frac{1}{v_2}\frac{\partial}{\partial t}\right)A_2 = -i\sigma_2 A_1^2 \exp\left[i\Phi(z)\right]-\gamma A_2^2 A_2^* \quad (14)$$

where A_1 and A_2 are the complex amplitudes of the fundamental and SH waves respectively and are functions of (z, t). The nonlinear coupling coefficients, $\sigma_{1,2}$, are calculated as $\sigma_{1,2} = 2\pi d_{eff,SHG}/(\lambda n_{1,2})$, where the magnitude of $d_{eff,SHG}$ for QPM waveguides is $d_{eff,SHG} = (2/\pi)d_{33}\beta$, and β is an overlap integral and is < 1. The parameter, $\gamma = (3\pi/4\lambda_2 n_2)\,\mathrm{Im}(\chi^{(3)})$ where $\mathrm{Im}(\chi^{(3)})$ is the imaginary part of the third-order nonlinear susceptibility[24]. The role of this term in the second equation of Eq. (14) is to account for the nonlinear losses observed in the experiments with both ppKTP and appKTP. The phase factor in system Eq. (14) is defined as $\Phi(z) = \Delta k_0 z$ for the ppKTP waveguide, and as before $\Phi(z) = \Delta k_0 z + D_g z^2$ for the appKTP waveguide.

In figure 3 we compare the analytical solution of Eq. (12) and Eq. (13) with the numerical solution of Eq. (14) for the SHG conversion efficiency for three different pulse profiles (hyperbolic secant, Gaussian and rectangular). It can be seen that the simplified model perfectly describes the process of SHG when $L > 5L_{nst}$. Further, the analytical model of Eq. (12) and Eq. (13), valid for samples much longer the nonstationary length L_{nst}, does not depend on the pulse shape.

The effects of two-photon absorption (TPA) of the SH wave are included in the second equation of Eq. (14), in the form of the parameter $\gamma = (3\pi/4\lambda_2 n_2)\,\mathrm{Im}(\chi^{(3)})$, in order to explain the imbalance of the conservation of energy at the waveguide output. Experimental observations[13] have shown that, for input fundamental pulse energies of around 60 pJ, the ratio of $(P_{1,out}+P_{2,out})/P_{1,in}$ reached 75%, where P_1 and P_2 are respectively the average powers of the fundamental and SH beams. As the exact value of $\mathrm{Im}(\chi^{(3)})$ for KTP at 430 nm is, to our knowledge, not available in the literature, we have used these measured nonlinear-type losses in energy to set the value of the parameter, γ, in the system of Eq. (14).

The theoretical curves obtained from the solution of Eq. (14), with $\gamma = 0.03L\sigma^2$, are shown later in figure 18. If we take $d_{eff,SHG}$ = 3.6 pm/V, the value of γ used in the calculation corresponds to a TPA coefficient of 3.8 cm/GW, which is close to the reported TPA coefficient of $KNbO_3$ (3.2 cm/GW)[25].

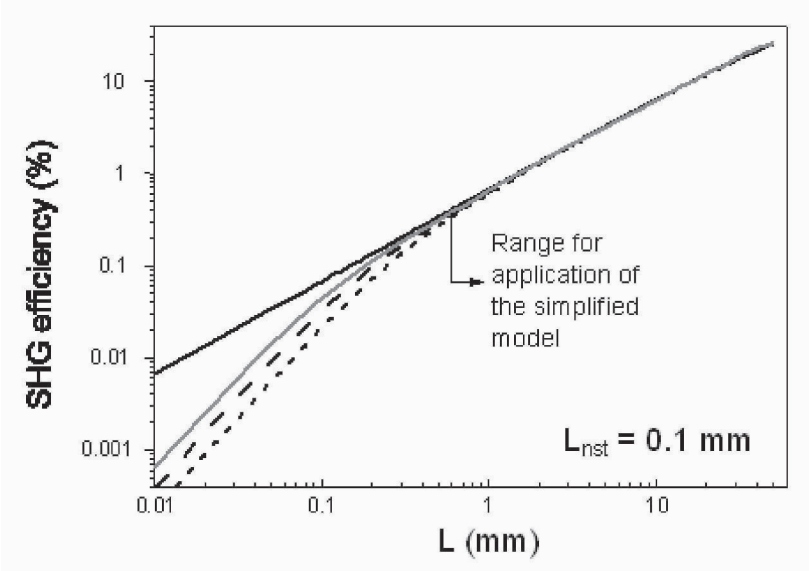

Figure 3. Comparison of simplified analytical solution for η_{cor} (black line) given by Eq. (13), and numerical solution of Eq. (14). Depletion effects are included for three different temporal pulse shapes: secant hyperbolic (gray line), Gaussian (dash line) and rectangular (short dash line). Nonlinear losses are neglected ($\gamma = 0$). Calculations are performed for a KTP waveguide with cross-sectional dimensions of 2 × 2 μm ($d_{\text{eff}} = 4.6$ pm/V). Input pulse energy is 1 pJ.

3. FABRICATION OF WAVEGUIDE CRYSTALS

Efficient nonlinear optical frequency conversion requires phasematching, large pump intensities, long interaction lengths and materials with large nonlinear optical coefficients. The limitations imposed on nonlinear optical mixing processes due to the low peak powers found in most quasi-cw and cw lasers can be overcome by creating waveguides in the nonlinear material.

The waveguide confines the beam, allowing for a high intensity over long interaction lengths. This can lead to a significant increase in the optical conversion efficiency, thus making guided wave nonlinear optical conversion ideal for applications requiring cw or low peak power quasi-cw lasers. Furthermore, efficient optical mixing throughout the entire transparency range of the crystal can be achieved by using a quasi-phasematched (QPM) process.

In a QPM nonlinear optical process, the waveguide is segmented into regions with alternating anti-parallel ferroelectric domains. For SHG, the

period of the domain grating for first order QPM is determined by the quasi-phasematching condition[26,27]:

$$\frac{n_2}{\lambda_2} = \frac{2n_1}{\lambda_1} + \frac{1}{\Lambda} \tag{15}$$

where Λ is the period of the domain grating, $\lambda_{1,2}$ and $n_{1,2}$ are respectively the wavelength and index of refraction of the fundamental and SH fields. For waveguides the index of refraction terms in Eq. (15) incorporate both the bulk properties of the crystal (as determined from the relevant Sellmeier equations) and the additional dispersion due to modal confinement in the waveguide.

The relationship between phasematched, non phasematched and quasi-phasematched interactions in the case of SHG is illustrated in figure 4. The quadratic curve shows the SHG growth for a phasematched process, while the sinusoidal curve represents the growth in the case of no phasematching. In a QPM process, when the fundamental and second harmonic fields are get out of phase, the periodically poled regions flip the phase of the second harmonic field allowing the SHG field to grow as it propagates through the crystal. In contrast to the usual birefringent phasematching, quasi-phasematched mixing processes can be exploited over the entire transparency range of the crystal.

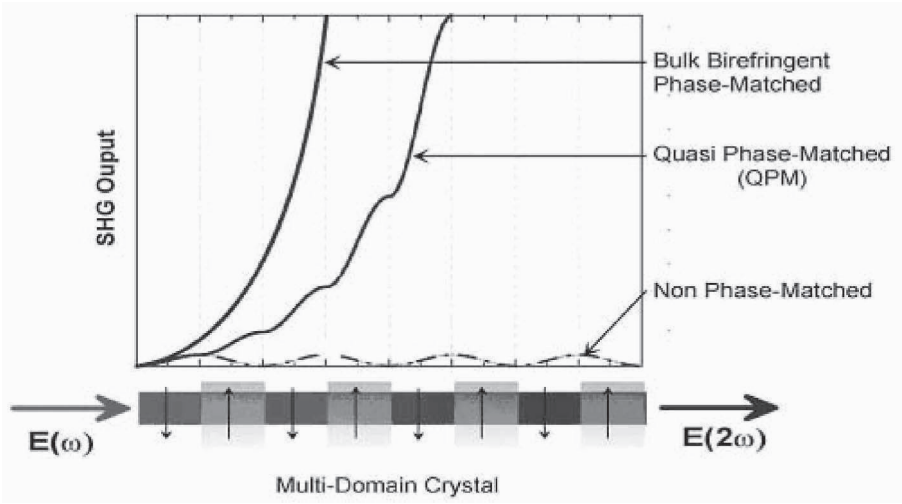

Figure 4. The graph shows the SHG output as a function of distance through a nonlinear crystal for various phase matching conditions.

The waveguides used in the experiments described in section 7 were fabricated using photolithography to transfer a mask containing the waveguide patterns to a KTP wafer and then using an ion-exchange process to embed the waveguides. The exact steps to fabricate the waveguides in a KTP wafer are outlined in figure 5 and are described in detail below.

The initial step is to layout the waveguide pattern using the *AutoCAD* software. The waveguide pattern is segmented, with the period of the segmentation equal to the required QPM period for SHG (e.g. for conversion of 850 nm the grating period is ~4 μm).

The waveguide pattern is transferred to the KTP substrate using photolithography as shown in the first four steps in figure 5. The first step in the photolithography process is to spin on a thin layer of photoresist that evenly covers the surface of a *z*-cut KTP substrate. The photomask, with waveguide design, is imaged onto the photoresist using a projection

Figure 5. The five steps required to transfer the waveguide pattern to the KTP substrate.

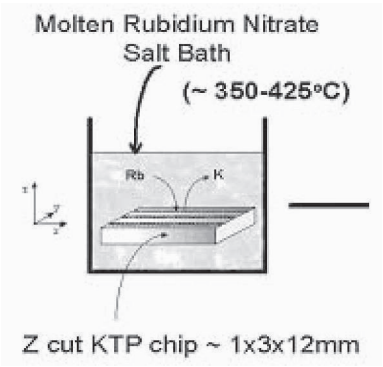

Figure 6. The illustration depicts the ion-exchange process that occurs in the oven.

lithography system. A developing process removes the exposed photoresist so only the unexposed regions of the KTP are covered. Next, a thin aluminum or SiO_2 coating is deposited onto the wafer. Submerging the wafer in acetone removes the remaining resist along with any aluminum (but not the SiO_2) in the exposed area creating a waveguide pattern.

The KTP chips are individually immersed in a molten bath of a mixture of $RbNO_3$ and $Ba(NO_3)_2$. Within this bath, the Rb ions diffuse into the unmasked portions of the KTP chip, while the K ions diffuse out of the substrate and into the bath, shown in the illustration in figure 6. In the diffused regions, the rubidium ions increase the index of refraction relative to the undiffused KTP and thus form the optical waveguide. Note that due to the presence of barium, there is an increase in the index of refraction and the ferroelectric domain in the diffused region is reversed and hence the term chemical poling is used for this process.

4. FABRICATION OF BULK CRYSTALS

4.1 Birefringent nonlinear crystals

The bulk potassium niobate ($KNbO_3$) crystal was grown using the top seeded solution growth (TSSG) method, which is one of the commonly used 'flux growth' techniques. In the TSSG method, the desired crystal is grown from a solvent containing the dissolved constituent components. Crystals are grown at a temperature below their melting point which prevents decomposition before melting or any unwanted phase transitions.

$KNbO_3$ is a ferroelectric crystal of the 'perovskite' family, which transforms from cubic to tetragonal, tetragonal to orthorhombic, and orthorhombic to rhombohedral phase at temperatures of 418°C, 203°C, and -50°C respectively. Once the bulk $KNbO_3$ crystal is slowly cooled down to room temperature to avoid unwanted cracks, it is then cut into blocks and poled by applying an electric field at a temperature just below the phase transition (~200°C) in order to generate a single domain. The required efficient phasematching interaction within such a nonlinear crystal has traditionally been accessed by exploiting the crystal's birefringence (as with $KNbO_3$). In general, however, this birefringent approach severely limits the flexibility in choice of nonlinear material and active wavelength.

4.2 Quasi-phasematched nonlinear crystals

The alternative is quasi-phasematching (QPM), where the desired crystal can be designed for a specific wavelength and fundamental spectral

bandwidth with an appropriate periodic structure. For the case of incident femtosecond pulses, characterized by significantly wider spectral bandwidths than continuous-wave sources, this is of particular interest as the spectral shape can be matched to the periodic structure. In addition, pulse shortening (or expansion) is possible by selectively arranging the different frequency converting regions. Finally a higher conversion efficiency can be obtained with QPM because the strongest nonlinear component, d_{33}, can be accessed, which is not the case for birefringent phasematching. Effective QPM has been demonstrated in many crystals, including $LiNbO_3$[28], $LiTaO_3$[29], RTP[30] and RTA[31], but we will concentrate here on KTP[32].

Periodically-poled KTP can be conveniently used at room temperature and can withstand high intensities without showing any sign of damage. The samples used in this work were made from flux-grown KTP, and the periodic structure was fabricated by electric-field poling according to the technology developed by Karlsson *et al*[32]. Flux-grown KTP can show substantial composition variations even though the optical properties are

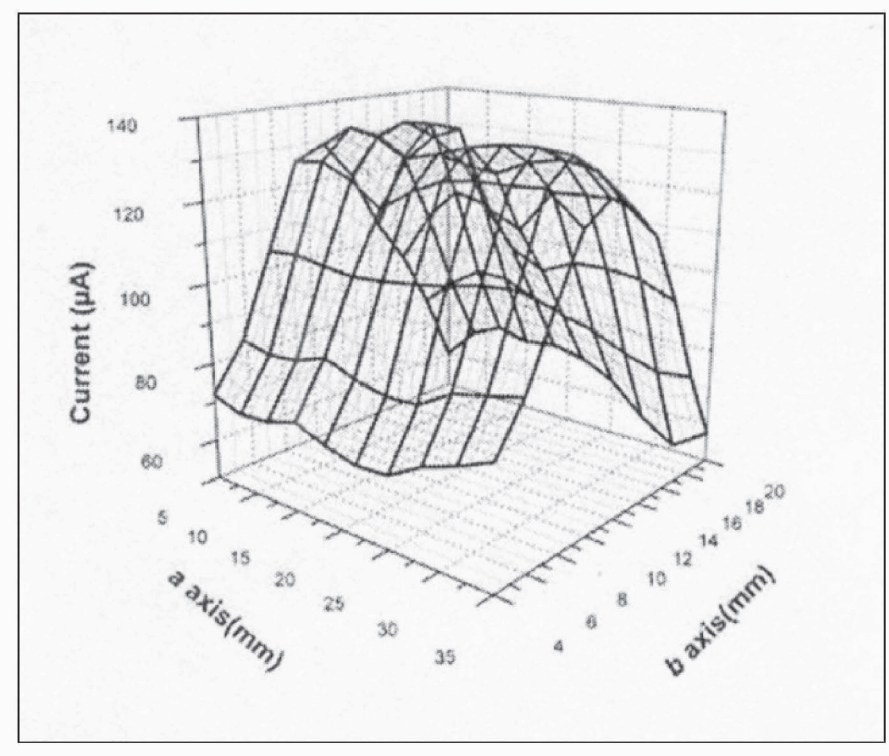

Figure 7. Conductivity map of KTP showing the ionic current variation over the wafer.

seen as identical. The composition variation, which is observed as a conductivity variation when an electric field is applied over the sample, can be detrimental for periodic poling. It is commonly seen that a sample with large degrees of such variations will result in three areas of composition, over poled, periodically-poled and unpoled regions. A typical conductivity map for a flux grown KTP wafer is seen in figure 7. As this figure illustrates, the change in conductivity (which can be as large as a factor of two) occurs mainly along the b-axis, whilst it is more or less constant along the a-axis.

The electric circuit used for the periodic poling as well as for the conductivity measurements is shown in figure 8. A high-voltage amplifier (*Trek 20/20C*) amplifies a waveform generated by an arbitrary signal generator (*Agilent 33120A*). The serial resistance of resistor R_1 limits the current passing through the sample during poling. The voltage over the sample is determined through the V_1, which is the voltage over R_3 and which forms a voltage divider parallel to the sample. By properly selecting the resistance R_2, the voltage is measured by an oscilloscope. The current through the sample is determined from the voltage V_2, which is the voltage over the small resistance R_4, in series with the sample. Resistances R_1, R_2, and R_3 are set as 15 kΩ, 100 MΩ, and 1.6 MΩ, respectively. R_4 was changed according to the measurement requirements. Contacts were made with a saturated solution of KCl.

During the spontaneous polarization reversal in an area, A, a charge of $Q = 2P_s A = \int i \cdot dt$ is deposited, which causes the poling current, i, to flow through the circuit. In low-conductivity ferroelectrics such as $LiNbO_3$ the domain inversion can be controlled by monitoring the current flowing in the poling circuit during the charge transport, and an integration of the current to determine the deposited charge over a specific area. However, for KTP the ionic conductivity is substantial in the *c*-direction at room temperature. The total measured current is then the sum of the poling current and the ionic current, and difficulties have arisen when attempting to separate these two contributions in order to obtain an accurate observation of the polarization switching process. The total current consists of two contributions, the ionic current, proportional to voltage U^2 and the poling current which rises sharply at voltages close to a coercive field. Ideally, the poling current should self-terminate as the whole area, A, under electrode is reversed.

To achieve better control of the poling, we have developed an on-line electro-optic monitoring technique[30]. The technique is based on the accumulated change of the electro-optic response when the domains grow through the crystal from the patterned side to the opposite side. A He-Ne beam polarized 45° to the z-axis is launched along the x-axis of the crystal (figure 9). When an electric field is applied, the output polarization state of

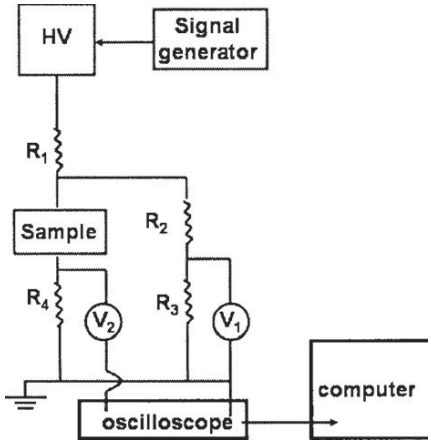

Figure 8. The electrical circuit used for all the polarization-switching experiments, as well as for the conductivity measurements.

the He–Ne beam will be changed due to the electro-optic effect. This results in a time dependent variation of the polarization state during the rise and the fall of the pulse. During the rest of the pulse, when the field is constant, the polarization state will be time dependent only if the sign of the electro-optic effect is reversed, i.e. the crystal is being poled.

The change of polarization state can be observed by measuring the intensity of the He-Ne beam through a polarizer orthogonal to the initial polarization. The intensity at the detector will then show a periodic oscillation during poling, which will stop when the poling starts (figure 9). When the poling parameters are chosen carefully, and when the crystal is homogeneous, only the area under the electrodes are poled, and no over-poling is obtained.

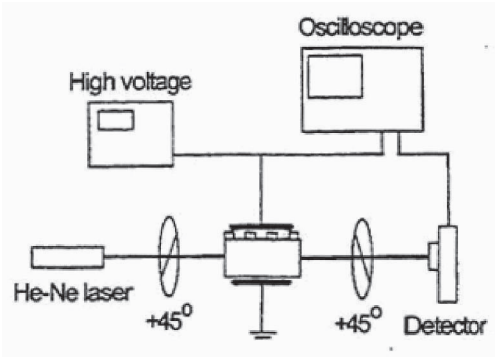

Figure 9. Schematic for monitoring the poling process[30].

Let us now concentrate on the specific sample used in this work. For the bulk appKTP crystal (used experimentally in section 7), the commercially-obtained KTP wafer was flux-grown, *c*-cut, single domain, 1 mm thick, and with the *c*-faces polished to an optical finish. For practical reasons, the wafers were cut into 10×5 mm^2 pieces after the conductivity measurements.

In flux-grown KTP, the ionic conductivity along the *c*-axis can vary by as much as an order of magnitude over a single wafer[33]. This was found to severely complicate the periodic poling. Thus, we first mapped the conductivity distribution on each wafer. Using the set-up of figure 8, 5-millisecond positive square electrical pulses of 1.5 kV in magnitude were applied to the c^--face of the wafer using an In-covered probe of 1 mm in diameter, while the c^+-face was uniformly contacted using a saturated solution of KCl. The probe was scanned over the wafer surface, measuring the ionic current through the resistor R_4, which was set to 10 kΩ.

A typical measured ionic-current map of a KTP wafer, which illustrates the conductivity distribution, is seen in figure 7. The measured current of 100 μA yields an absolute value of the conductivity at 1 mm^2 of about 8.5×10^{-7} S/cm. It shows a parabolic variation along the b-axis, increasing by a factor of 2 from to the edges to the center, whereas it remains almost constant along the *a*-axis. The concentration of K^+ vacancies, which is the main contributor to the ionic conductivity, is very sensitive to crystal growth temperature. Thus, the variations in conductivity over the KTP wafer are most probably due to a temperature gradient during crystal growth that results in a spatially varying stoichiometry. In this work, samples with low conductivity from the edge of the wafer whose conductivities are relatively low (7×10^{-7} S/cm) were chosen. To get even more homogeneous conductivity and to get good nucleation for domain reversal we ion-exchanged the sample in pure $RbNO_3$ for 6 hrs at 350˚C. Rb is then diffusing into the surface layer of the crystal replacing K and filling K-vacancy positions[32]. The reduction in conductivity is a consequence of the larger ionic radius of Rb in the KTP lattice. These atoms will hence drift more slowly through the crystal in the applied field, which is the same as having a lower ionic conductivity. The Rb ion exchange is faster in regions of higher K-vacancies (higher conductivity) and this will then help to make the material more homogeneous in conductivity and hence improve the periodic poling. A second advantage of the ion-exchange is that the crystal will have a thin low conductive layer (a few μm) on the surface which then will take a corresponding larger part of the electric field when voltage is applied over the sample. The domains will nucleate in this layer and then propagate through the bulk of the sample to the opposite side again helping creation of a periodic domain structure of high quality.

The sample was patterned with periodic photoresist using conventional photolithography. In the poling the photoresist works as an isolator on the sample surface and the area under the mask will stay un-inverted while the areas under the openings are the regions that will be inverted during periodic poling. The back-side of the sample was coated with an Al film to prevent depletion of K from the sample during the following E-field poling.

The sample, with patterned area of 4×4 mm^2 was contacted with $KCl:H_2O$ liquid electrodes, and two 2.2 kV pulses (6 ms long) were applied. The sample was then tested in an SHG experiment and the back metal electrode and the photoresist was removed.

In order to write the periodic structure onto the KTP crystal, a photolithographic mask was constructed. Conventional masks have a single-grating period, typically ranging from 3.4 μm to 3.6 μm for first-order QPM applications, which is patterned over the whole length of the crystal[28-32]. In recent years, paralleled with improvement of e-beam and UV-laser lithography technologies, novel grating structures have appeared, such as multi-gratings, Fibonacci sequenced gratings, and aperiodic (chirped) gratings[34-36]. For the case of aperiodically-poled gratings, a linear chirp is deployed over a mask with length L, having a starting period of Λ_s and an ending period of Λ_f. The chirp parameter, α, is then simply calculated from $\alpha = (\Lambda_s - \Lambda_f)/L$. In our case the manufactured mask length had a length of L = 4 mm, with a starting and ending period of Λ_s = 4.1 μm and Λ_f = 4.3 μm, respectively, and a chirp-parameter of α = 0.05. These parameters are valid for an idealized linear chirp. However, when manufacturing the actual grating the limiting factor is the resolution of the lithographic process; for our chirped grating a resolution of 0.05 μm was used.

5. PORTABLE FEMTOSECOND INFRARED LASER

Our recent investigations into efficient frequency-doubling of femtosecond pulses in waveguide and bulk nonlinear crystals have allowed us to propose the design of a portable ultrafast blue light source[11], which takes advantage of a previously reported ultra-compact femtosecond Cr:LiSAF laser design[10,37-40]. The extremely low pump-threshold conditions (~22 mW to sustain modelocking) associated with this Cr:LiSAF laser permit the use of inexpensive (~US$40) single-narrow-stripe AlGaInP red laser diodes (50-60 mW) as a pump source[41]. Their modest electrical drive requirements (~100 mA current, ~200 mW electrical power) mean that these diodes require no active electrical cooling and can easily be powered for a number of hours by regular 1.5 V penlight (AA) batteries. With a maximum pump power from two pairs of pump laser diodes of ~200 mW, the

Cr:LiSAF laser crystal does not require any cooling. As a result, relatively inexpensive femtosecond Cr:LiSAF lasers with optical output powers up to 45 mW, robustly modelocked with a semiconductor saturable absorber mirror (SESAM), are achievable from entirely self-contained and portable units with dimensions of 22 cm × 28 cm. [A version of this laser design incorporating one pair of pump laser diodes is shown in figure 10] A second pair of pump laser diodes can easily be incorporated onto the baseplate to maximize operational performance (figure 12).

The modest electrical drive requirements of these diodes, and the resulting option to power the laser with standard penlight (AA) batteries, allow these Cr:LiSAF lasers to boast an impressive electrical-to-optical efficiency of over 4 %, which until recently[42] was the highest reported overall system efficiency of any femtosecond laser source. The amplitude stability of the laser output was observed to be very stable with a measured fluctuation of less than 1% for periods in excess of 1 h. These measurements were made on a laser that was not enclosed and located in a lab that was not temperature-controlled. In a more enclosed and controlled local environment we would expect the amplitude fluctuations of this laser to be extremely small. While the output powers achievable from these lasers have been limited by the available power from the AlGaInP red laser pump diodes, there are already strong indications that commercial access to higher-power suitable diode lasers is imminent.

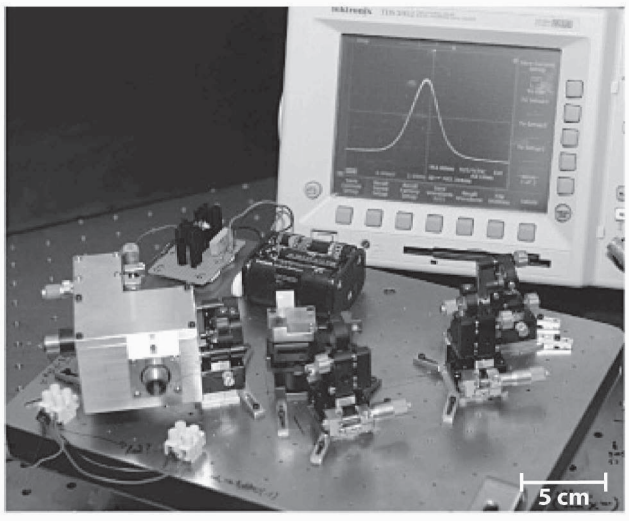

Figure 10. Photograph of ultra-compact, portable femtosecond infrared laser pumped by two inexpensive (~US$40) single-narrow-stripe AlGaInP diodes and powered by standard penlight (AA) batteries[10]. An oscilloscope in the background records an intensity autocorrelation of the femtosecond pulses.

6. SIMPLIFIED SECOND HARMONIC GENERATION SCHEME

By incorporating a straightforward but highly efficient frequency-doubling scheme into the compact femtosecond infrared laser of figure 10, a portable ultrafast blue light source can be achieved. To generate blue light (~425 nm), all that is required is a single extracavity lens to focus the ~850 nm light from a Cr:LiSAF laser through a nonlinear frequency-doubling crystal in a single pass configuration (figure 11). A half-wave plate (HWP) may also be required to select the appropriate linear polarization.

The phasematching conditions of all four doubling crystals investigated in this paper comfortably allow efficient and optimal blue-light generation at room temperature. In addition, the phasematching acceptance bandwidths (which define the accuracy to which the crucial parameters of nonlinear crystal temperature, fundamental wavelength and incident angle must be maintained to successfully optimize the SHG process) are sufficiently relaxed to require minimal attention once the process has been optimized. Each nonlinear crystal is mounted on a basic thermoelectric cooler (TEC) which provides some current-controlled temperature stabilization should it be required.

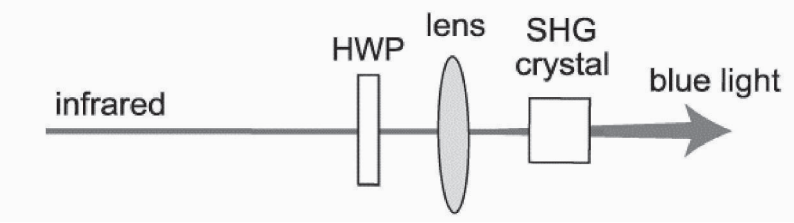

Figure 11. Simplified efficient blue generation scheme. A single pass of pulsed infrared light through an extracavity lens and nonlinear crystal is all that is required. A half-wave plate (HWP) may also be included if necessary.

7. EXPERIMENTAL PERFORMANCE OF WAVEGUIDE AND BULK NONLINEAR CRYSTALS

Investigations into the relative performance of the four nonlinear crystal types were carried out using the femtosecond Cr:LiSAF laser illustrated in figure 12. Although this laser configuration differs slightly from the laser configuration of figure 10 (with an extra pair of pump laser diodes for increased output power[10], and an intracavity prism to allow wavelength

tuning), these modifications do not compromise the small scale or potential portability of the laser construction.

With four single-narrow-stripe pump laser diodes (two providing up to 60 mW at 685 nm, and two providing up to 50 mW at 660 nm) the laser was capable of generating 120-210 fs pulses at a repetition-rate of 330 MHz and average output powers up to 45 mW. By simply tilting the angle of the output coupler, selection of the central operating wavelength was also possible between 825 nm and 875 nm (defined by the reflectivity bandwidth of the SESAM mirror). The infrared output beam was strongly linearly polarized (due to the Brewster surfaces of the Cr:LiSAF laser crystal) and the beam quality was measured to have an $M^2 = 1.1$. The stability of the pulsed output over a number of hours was observed to be excellent, together with negligible power degradation.

Each nonlinear crystal was assessed in an extracavity single-pass arrangement at room temperature (figure 11). A half-wave plate was required for certain nonlinear crystals to provide the correct linear polarization. The relative performance of the four nonlinear crystals is summarized below in sections 7.1 to 7.4.

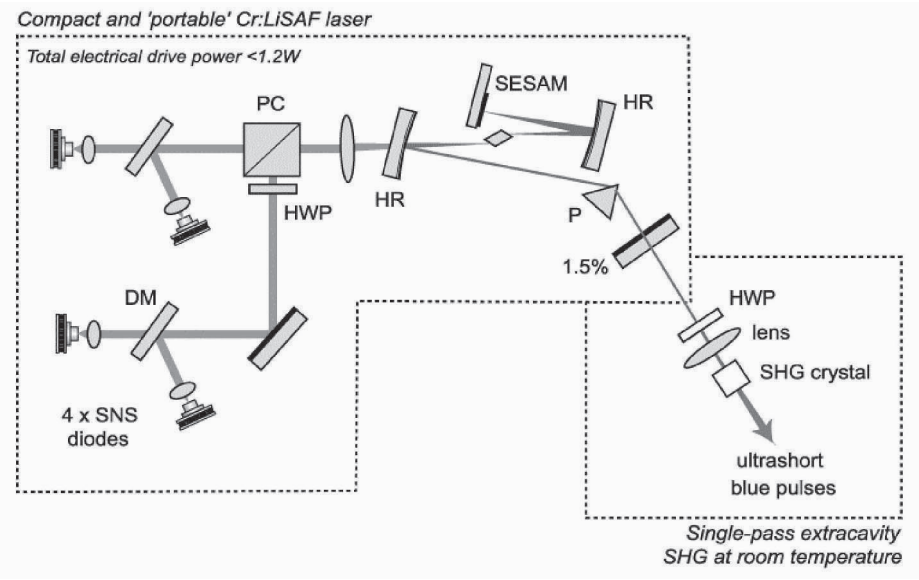

Figure 12. Laser configuration for SHG experiments, incorporating four single-narrow-stripe (SNS) red laser diodes and a prism (P) for wavelength tuning (DM: dichroic mirror; HWP: half-wave plate; PC: polarization cube; HR: high reflector; 1.5 %: output coupler).

7.1 Bulk $KNbO_3$

Bulk potassium niobate ($KNbO_3$) is well suited to our needs, because birefringent type-I non-critical phasematching (NCPM) can be exploited for highly efficient SHG of ~850 nm at room temperature[12,16,17]. This NCPM avoids any spatial walk-off between the fundamental and second harmonic beams, as well as maximizing the angular acceptance of the phasematching process.

Using an experimentally-optimized focusing lens (f = 15 mm; spot radius, w = 4.3 μm) and a 3 mm $KNbO_3$ crystal (cut for NCPM at 22°C and 858 nm; AR-coated), up to 11.8 mW of blue average power with a spectral width up to $\Delta\lambda_{SH}$ = 1.4 nm at 429 nm was generated with only 44.6 mW of incident fundamental. The maximum observed SHG conversion efficiency was as high as 30 %. The overall efficiency of the electrical-to-blue process was over 1 %, and the blue pulses were measured by autocorrelation to be ~500 fs in duration[12].

The measured full-width-at-half-maximum (FWHM) wavelength and temperature acceptance bandwidths were 2.7 nm and 5 °C respectively. The beam quality parameter of the generated femtosecond blue beam was observed to be M^2 = 1.8. We believe the quality of the blue beam deteriorated slightly from the fundamental beam (M^2= 1.1) as a result of the strong focusing. Because exact phasematching conditions are satisfied only at the beam centre, peripheral rays propagate under conditions of slight mismatch and as such accumulate phase distortions.

7.2 Waveguide ppKTP

Potassium titanyl phosphate (KTP) is another suitable nonlinear crystal for SHG, given that it can be waveguided and periodically-poled to readily satisfy quasi-phasematching (QPM) conditions at room temperature. This waveguide ppKTP crystal, periodically-poled for SHG of ~850 nm and not AR-coated, had cross-sectional dimensions of ~4×4 μm in diameter and was 11 mm in length (including a 3 mm Bragg grating section[43] which did not affect the performance of the Cr:LiSAF pump laser).

With an appropriate aspheric lens (f = 6.2 mm) to optimize the coupling of the fundamental light into the waveguide, up to 5.6 mW of average output blue power with a spectral width of $\Delta\lambda_{SH}$ = 0.6 nm at 424 nm was achieved for 27 mW of incident fundamental. Accounting for a coupling efficiency of 70%, the associated internal SHG conversion efficiency within the waveguide was calculated to be as high as 37 %[13]. With the Cr:LiSAF laser requiring no more than 1.2 W of electrical drive, this corresponds to an overall electrical-to-blue system efficiency of 0.5 %. Evidence of a

saturation and subsequent decrease in overall efficiency of the SHG process (figure 18) has been attributed to two-photon absorption of the second harmonic (SH) wave[13]. The superiority of the ppKTP waveguide at low pulse energies is evident when comparing the slope efficiency per unit length of this experimental data (6.9 %$pJ^{-1}cm^{-1}$) with other similar SHG experiments using bulk $KNbO_3$ (1.0 %$pJ^{-1}cm^{-1}$ [16], 0.73 %$pJ^{-1}cm^{-1}$ [12]) and waveguide ppKTP (0.15 %$pJ^{-1}cm^{-1}$ [44]).

A broad temperature acceptance bandwidth of $\Delta T \sim 30$ °C (FWHM) centered at 18 °C easily permitted room-temperature operation. The characterization of fundamental pulses entering ($\Delta\tau \sim 170$ fs; $\Delta\nu\Delta\tau \sim 0.32$) and leaving ($\Delta\tau \sim 195$ fs; $\Delta\nu\Delta\tau \sim 0.37$) illustrated that these pulses were dispersed only slightly on propagation through the waveguide.

7.3 Bulk appKTP

While periodically-poled materials are typically characterized by very narrow spectral acceptance bandwidths (< 1 nm), aperiodically-poled structures (characterized by a linear gradient in grating period) have the advantage of providing sufficiently broad spectral acceptance bandwidths to utilize more of the spectrum associated with picosecond[45] and femtosecond[46] pulses. They can also simultaneously provide some pulse compression of sufficiently pre-chirped incident pulses[22,23].

The bulk appKTP crystal was 4 mm in length, and was not AR-coated. The grating periods varied from 4.1 μm to 4.3 μm in order to provide a fundamental bandwidth of 7 nm, for SHG at room temperature centered at 851 nm. With an experimentally-optimized focusing lens (f = 15 mm; w = 4.3 μm), 3.2 mW of blue average power was produced at 429 nm with $\Delta\lambda_{SH}$ up to 1.4 nm, from 27 mW of incident fundamental. This corresponds to an SHG conversion efficiency of 11.8 %, and an overall electrical-to-optical system efficiency of 0.3 %. The wavelength acceptance bandwidth was measured to be 4.5 nm. In attempting to measure the temperature acceptance bandwidth, a negligible deterioration in SHG efficiency was observed when adjusting the bulk appKTP crystal temperature between 10°C and 50°C.

Although the absolute efficiency of the SHG process is lower than that achieved from the $KNbO_3$ crystal, figure 13a illustrates that, either with suitable pre-chirping of the fundamental pulses or recompression of the generated blue pulses, the bulk appKTP crystal is able to provide ultrashort blue pulses with higher peak powers, P_{pk} [$P_{pk} = E_p/\Delta\tau_{SH}$, E_p is the pulse energy and $\Delta\tau_{SH}$ is the second harmonic pulse duration]. Insufficient power was available to measure $\Delta\tau_{SH}$ from the bulk appKTP crystal, but $\Delta\tau_{SH}$ for our experimental conditions was calculated to be ~370 fs, with ~270 fs

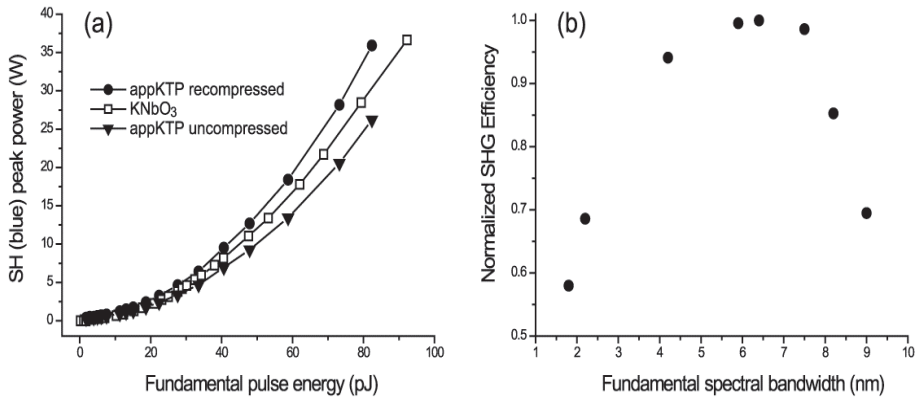

Figure 13. (a) Relative blue pulse peak powers from bulk appKTP and bulk KNbO3 crystals. (b) Dependence of SHG efficiency on fundamental spectral bandwidth of femtosecond Cr:LiSAF laser.

possible with suitable compression. The data for the $KNbO_3$ crystal used in figure 13a was calculated using measured values of $\Delta\tau = 540$ fs and $\Delta\nu\Delta\tau = 0.39$[12].

The bulk appKTP crystal is the least impressive of the four nonlinear crystals in terms of absolute SHG efficiency (figure 20). While the nonlinear coefficient, d_{eff}, of KTP (7.8 pmV^{-1}) is less than that of $KNbO_3$ (12.5 pmV^{-1}), an additional explanation is evident from figure 13b, which is measured for constant fundamental pulse energy. This clear dependence of SHG efficiency on fundamental spectral bandwidth (broadened by the insertion of more glass from the intracavity prism in figure 12) is surprising, given the fact that the bulk appKTP crystal was designed for broad fundamental pulses ($\Delta\lambda$ ~7 nm). However, the single-pass SHG scheme of figure 11 allows tight focusing of the fundamental beam in the centre of abulk nonlinear crystal in order to generate sufficiently high intensities for efficient nonlinear conversion. Although the aperiodic structure in the bulk appKTP crystal varied from 4.1 μm to 4.3 μm over a length of 4 mm, the associated confocal parameter (estimated to be the distance over which SHG takes place) is only 0.3 mm. Therefore, in the case of such tight focusing, the fundamental field will not experience the full gradient of the aperiodic structure. As such, the effective fundamental bandwidth is narrowed. The optimum 7 nm bandwidth indicated by figure 13b represents an expected expansion of the wavelength response due to the broadband fundamental.

7.4 Waveguide appKTP

The need for tight focusing in the bulk appKTP crystal (above) at relatively low power levels (~30 mW) resulted in some narrowing of the available phasematching bandwidth. This is easily avoided by using a waveguided structure, where the full aperiodicity of the appKTP structure can be utilized.

The waveguide appKTP crystal had cross-sectional dimensions of ~4 × 4 μm, and length of 12 mm. The waveguide, which was not AR-coated, was designed for single-mode transmission, and for a fundamental bandwidth of 11 nm (i.e. for SHG of 839 – 851 nm). The linear grating chirp is represented by a change in grating period from 3.8 μm to 4.0 μm.

With a suitable coupling lens of 6.2 mm focal length, up to 5.4 mW of blue average power at around 422 nm was obtained from 24.8 mW of fundamental. The internal SHG efficiency reached a maximum of 32 %, with an overall system electrical-to-blue efficiency of 0.4 %. The effects of utilizing the full aperiodicity of the appKTP waveguide structure was evident when observing the generated blue spectral bandwidths. Whereas the bulk appKTP crystal provided blue spectra with bandwidths of around 1 nm, broader blue spectra up to ~2.5 nm were observed (figure 14b), which supported shorter duration blue pulses. The structured oscillatory nature of the blue spectral profile, also recently observed elsewhere[47], is discussed in section 8.2.

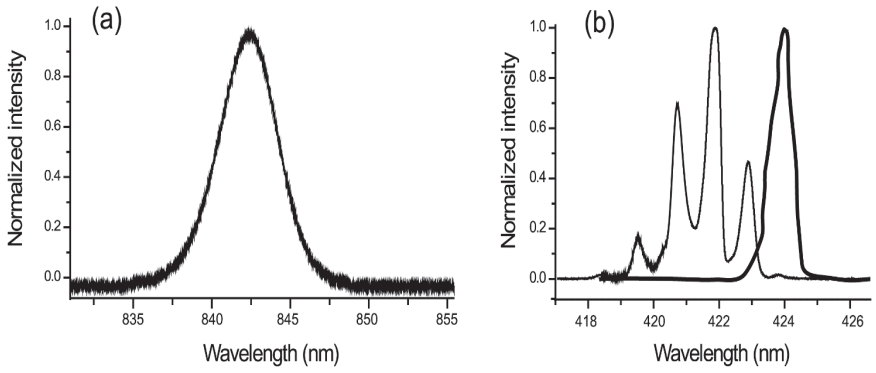

Figure 14.(a) Spectrum of fundamental pulses transmitted through the appKTP waveguide crystal (Δλ ~5 nm). (b) Typical structured spectra of the second-harmonic blue pulses leaving the appKTP waveguide, with a FWHM spectral bandwidth of up to approximately 2.5 nm (*thin line*); and typical unstructured spectra of the second-harmonic blue pulses leaving the appKTP bulk crystal (thick line).

Tunability of the blue light from 418 nm to 429 nm was also possible, via simple tuning of the Cr:LiSAF pump laser. This 11 nm tuning range coincides with the fundamental acceptance bandwidth of 11 nm for which the appKTP waveguide was designed.

8. COMAPARISON OF EXPERIMENTAL RESULTS WITH THEORETICAL MODELS

8.1 Bulk nonlinear optical crystals

In modeling the SHG performance of the bulk nonlinear optical crystals, we have assumed the incident fundamental pulses are characterized by a hyperbolic secant temporal profile, and therefore $\tau = \tau_{\text{fund}}\,(\text{FWHM})/1.76$. For the case of $KNbO_3$, the maximum optical-to-optical SHG efficiency achieved was 30%. The corresponding value of L/L_{nst} under these conditions, with a GVM parameter, α_{KNbO3} = 1.2 ps/mm, is L/L_{nst} = 30. The values of beam waist, w_{01}, and confocal parameter, b, are calculated from conventional ABCD matrices using the measured beam diameter, d, before the focusing lens. The experimental uncertainties in the determination of w_{01} and b are 5% and 10% respectively.

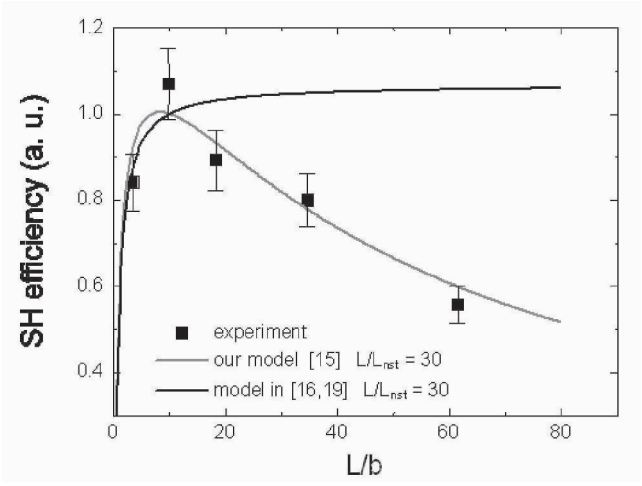

Figure 15. Experimental values of SHG efficiency using the bulk $KNbO_3$ crystal (data points), and the predictions of our model (gray curve)[15] and another model (black curve)[16,19] for L/L_{nst} = 30, as a function of the focusing strength, $m = L/b$. The theoretical curves are normalized to their values for L/b = 10, which was the experimental optimal focusing strength[12]. The maximum experimental point refers to a SHG efficiency of 30%.

In figure 15 we show the experimental values of normalized SHG efficiency as a function of the focusing strength, $m = L/b$. The experimental data is plotted together with theoretical predictions from our model described here, as well as the model published in references[16,19]. Both models assume the ratio $L/L_{nst} = 30$, and both theoretical curves are normalized for $L/b = 10$. We see from figure 15 that our model describes correctly the existence of a maximum in the dependence of SHG efficiency on focusing strength. To determine whether our model predicts the absolute efficiency, we have made use of the initial part (< 20%) of the experimental data. Working with different published values for the second order nonlinearity constant, d_{32}, of $KNbO_3$[48-50] we find that the corrected value of $d_{32} = 12.5$ pm/V published in reference[49] gives the best agreement not only with the experiment reported here, but also with the experimental work published previously[16,19].

Fitting the experimental data from the $KNbO_3$ experiment with Eq. (8), we find an experimental value of η_{slope} = 0.30 %pJ^{-1}, whereas the theoretical value from Eq. (6) is η_{slope} = 0.32 %pJ^{-1} (using d_{eff} = 12.5 pmV^{-1}, τ_0 = 210 fs and, from the model[15], a calculated value of h_{tr} = 0.137). The agreement is illustrated in figure 17. We consider this agreement between experiment and theory to be very good, taking into account that the theoretical values are calculated from the empirically-determined τ_{fund} and b which have a 10% error margin. The agreement for the lengthening of the SH pulse, τ_{SH}/τ_{fund}, is also excellent, as can be seen from $(\tau_{SH}/\tau_{fund})_{EXP} = 2.6$ and $(\tau_{SH}/\tau_{fund})_{THEORY} = 2.4$. At this point we would like to note that the model described by Weiner and Yu[16,19] cannot explain the change in SH pulse durations. This is because these models are built on the restricting assumptions of unchanging pulse shapes and constant duration for both interacting waves.

Experimentally, it was not possible to measure the dependence of the SH pulse duration on focusing strength due to the low sensitivity of the pulse duration measurement system. Instead, the dependence of the SH pulse spectral width was measured as a function of focusing strength. In figure 16 the experimentally measured narrowing of the SH spectral width with an increase of ratio b/L is compared with the theoretical prediction from our model. To plot the theoretical curve in figure 16 we have assumed transform-limited pulses with a temporal profile given by $\Delta f_{fund}/\Delta f_{sh} = \tau_{sh}/\tau_{fund}$. Due to the presence of GVM, the increase in the confocal parameter, b, leads to a broadening of the SH pulse, and therefore to a narrowing of the SH spectra. On the other hand, for very small values of the confocal parameter, b, the SHG process is stationary and the transformation of the spectra behaves as if in the long-pulse limit. We can see that the model presented here also describes the spectra of the generated

SH pulses, although the presumption that the SH pulses have a hyperbolic secant temporal profile is quite approximate. Correct accounting of the SH pulse shape would improve the accuracy of the model even further. Significantly, the model reported in references[16,19] is not able to describe such a dependence for the reasons discussed above. Although our analysis has assumed fundamental pulses with no frequency chirp, it is possible to extend the present model to describe SHG with chirped fundamental pulses.

In another study of SHG in the femtosecond regime, an experiment to determine the optimal focal position within a bulk $KNbO_3$ crystal has been carried out[17]. It was shown that, at low powers below the saturation regime, the optimal position of the focal spot is indeed in the center of the crystal as predicted by our present model.

Fitting the experimental data for the bulk appKTP crystal to Eq. (8), we obtain the experimental value $\eta_0 = 0.16\ \%pJ^{-1}$. From Eq. (6) we calculate the theoretical value of $\eta_0 = 0.16\ \%pJ^{-1}$ (using $d_{eff} = 7.8\ pmV^{-1}$, $\tau_0 = 210$ fs and a calculated value of $h_{tr} = 0.087$). Once again, figure 17 illustrates the accuracy of the model to experimental observations.

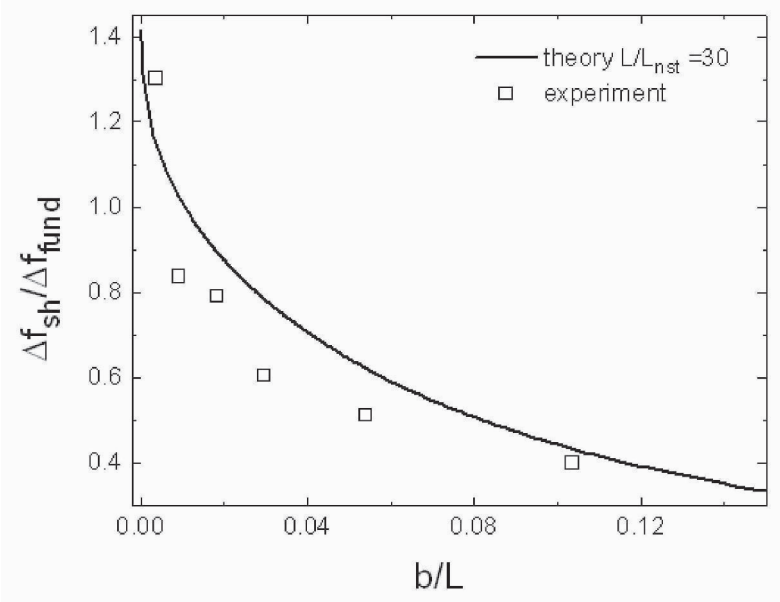

Figure 16. Experimentally measured evolution of the SH pulse spectral width relative to the fundamental spectral width for the bulk $KNbO_3$ crystal (data points), and the theoretical prediction of our model calculated for $L/L_{nst} = 30$, as a function of the ratio b/L[15].

It is worth repeating that the relatively low efficiency for the appKTP crystal is due to the fact that d_{eff}(KTP) < d_{eff} ($KNbO_3$). Performing the same assessment with lithium niobate ($LiNbO_3$) should yield up to four times the efficiency, because d_{eff} ($LiNbO_3$) = 17.6 pmV^{-1}. Unfortunately, insufficient power was available to measure the duration of the blue pulses from the bulk appKTP crystal. However, our calculations show that the generated blue pulses would be characterized by an uncompensated duration of 370 fs. These pulses could be compressed to around 270 fs in order to access higher peak powers.

8.2 Waveguide nonlinear optical crystals

When using the waveguide ppKTP crystal experimentally, the dependence of internal SHG efficiency on input power is characterized by a maximum efficiency of 37 %. A further increase in fundamental pulse energy then leads to a saturation and subsequent decrease in the efficiency of the SHG process (figure 18). This behavior was also observed in the waveguide appKTP crystal (figure 18), and has been reported elsewhere[44,47]. As we have suggested previously[13], two-photon absorption (TPA) of the second-harmonic (SH) wave is the most likely explanation for this behavior.

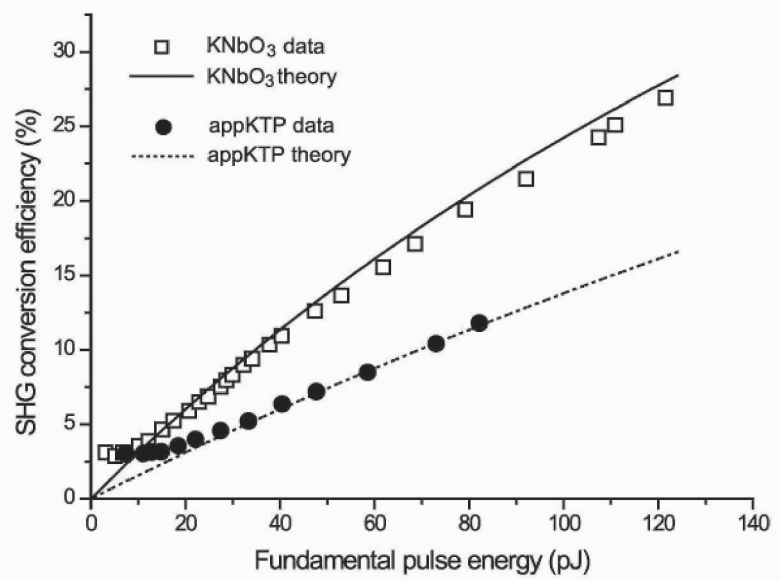

Figure 17. Theoretical predictions versus experimental data for the performance of the bulk nonlinear crystals, $KNbO_3$ and appKTP.

In figure 18 we also provide theoretical curves for the performance of the waveguide crystals, which account for the observed effects of TPA. The horizontal scales are normalized to match the initial slopes of the experimental curves. It is clear that the presence of TPA causes the slight decrease in SHG efficiency once saturation of the SHG process has begun. The fact that the measured efficiency is less than that predicted by the theory shows that the model can be improved further. This could be achieved by accounting for other effects such as nonlinear losses of the SH wave due to presence of the fundamental wave, self-phase and cross-phase modulation and blue-light induced red absorption (BLIRA)[25,51]. Thermally-induced phase mismatch may also be present as the blue wavelength is close to the absorption edge of the crystal.

Theoretical output spectra for the fundamental and SH waves for the appKTP waveguide are shown in figure 19. It can be seen that they closely represent the observed experimental oscillatory nature of the SH spectra, and the smooth profile of the fundamental output, as shown in figure 14. Our calculations predict that the oscillations in figure 19b become more exaggerated as we tune away from the perfect phasematching condition. In addition, the calculated acceptance bandwidth for our waveguide appKTP crystal of $\Delta\lambda_{fund}$ = 12.6 nm is in excellent agreement with the tests carried out on the sample after fabrication.

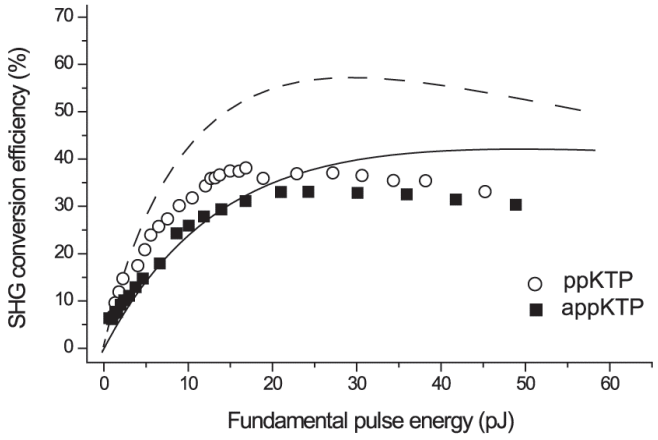

Figure 18. Saturation of SHG efficiency in the waveguide (ppKTP and appKTP) experiments (point data). Theoretical predictions incorporating the effects of two-photon absorption for the SH wave and group velocity mismatch are also shown for the ppKTP (dashed line) and appKTP waveguides (solid line).

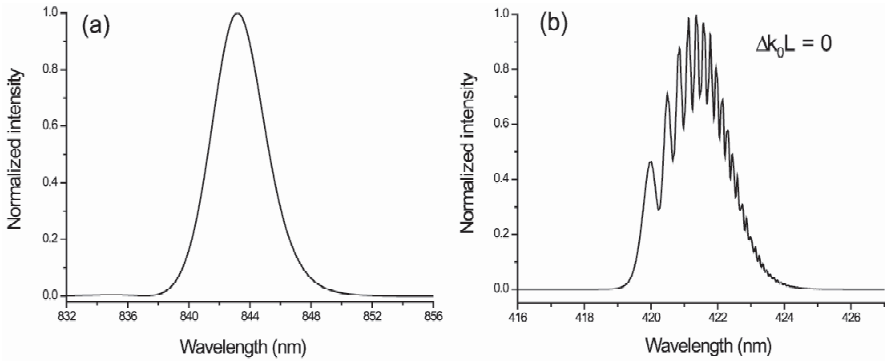

Figure 19. Theoretically calculated output spectra for (a) the fundamental and (b) second harmonic wave. See figure 14 for experimental spectra.

9. DISCUSSION AND SUMMARY

Of the four nonlinear crystal types investigated in this paper (figure 20), bulk $KNbO_3$ was superior in terms of generated blue average power (11.8 mW) and generated beam quality. $KNbO_3$ is also less susceptible to the observed saturation and subsequent decrease in SHG efficiency observed in both waveguide crystals.

The appKTP waveguide provided similar maximum internal SHG efficiency (32 %) to that of a ppKTP waveguide (37 %), and the steep rise in SHG efficiency proves the effectiveness of such waveguides under low pump-pulse-energy conditions. In addition, the broad wavelength acceptance bandwidth of the appKTP waveguide enabled the blue pulses to be tuned from 418 nm to 429 nm by frequency tuning of the Cr:LiSAF laser.

Blue spectral widths of up to ~2.5 nm and corresponding theoretical analyses confirm that significantly shorter blue pulse durations are obtained when aperiodic poling rather than periodic poling is used. As a result, higher peak power blue pulses can be generated with the bulk and waveguide appKTP crystals. Bulk appKTP is not ideally suited to low-power sources that require tight focusing to access sufficiently high intensities, although another advantage is the absence of efficiency saturation. Conveniently, all four crystals perform well at room temperature such that minimal wavelength and temperature stabilizations are required.

The theoretical model of SHG with focused beams in both homogeneous and linearly-chirped aperiodically-poled structures predicts very well the results from the bulk $KNbO_3$ and bulk appKTP crystals. The model of SHG in the two waveguide crystals explains qualitatively the saturation and

subsequent decrease of the SHG efficiency, but requires further refinement to explain more fully the experimentally-observed absolute efficiency.

The advantages of using bulk, waveguide, periodically-poled or aperiodically-poled media can be exploited with the intended application in mind. The relative performance of the four nonlinear crystals is summarized in Table 1.

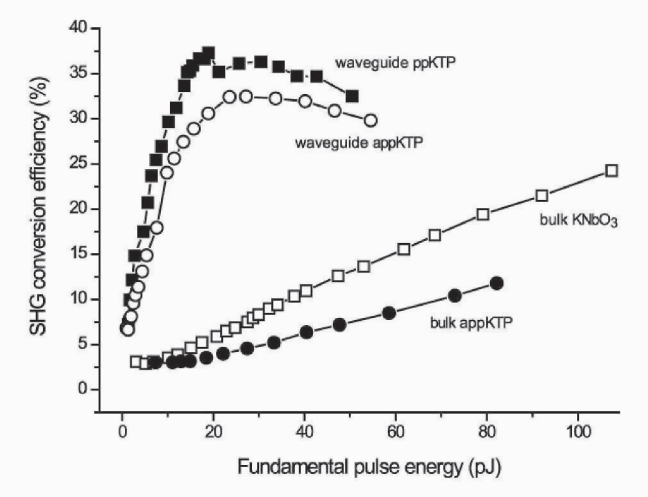

Figure 20. Relative experimental performance of the four nonlinear crystals investigated in this paper as a means to efficiently and practically generate ultrafast blue light from a compact and portable femtosecond Cr:LiSAF laser.

Table 1. Summary of the performance of the four nonlinear crystals

	bulk $KNbO_3$	waveguide ppKTP	bulk appKTP	waveguide appKTP
L	0.3	0.8	0.4	1.2
α	1.2	1.2	1.2	1.2
b	0.31	-	0.25	-
f	15	-	15	-
P_{SH}	11.8	5.6	3.2	5.4
η_{SHG}	30	37	12	32
η_{slope}	1	6.9	0.4	2.3
Ep_{SH}	36	17	10	16
$\Delta\lambda_{SH}$	<1.4	0.6	<1.4	~2.5

L: nonlinear crystal length (cm); α: GVM parameter ($ps.mm^{-1}$); *b*: confocal parameter (mm) ; *f*: focal length (mm); P_{SH} : blue average power (mW); η_{SHG}: maximum SHG conversion efficiency (%); η_{slope}: SHG slope efficiency per unit crystal length ($\%pJ^{-1}cm^{-1}$); Ep_{SH}: blue pulse energy (pJ); $\Delta\lambda_{SH}$: blue spectral bandwidth (nm).

10. CONCLUSIONS

We have performed a thorough experimental and theoretical investigation into efficient frequency-doubling of low energy femtosecond pulses. Evaluation of periodically-poled and aperiodically-poled bulk and waveguide structures has been presented. Several theoretical models accurately describe the temporal and spectral properties of the generated second harmonic (blue) light, as well as the observed saturation behavior of the conversion process. All experimental evaluations have been carried out with a potentially portable, diode-pumped femtosecond Cr:LiSAF laser.

ACKNOWLEDGEMENTS

Ben Agate acknowledges support from the UK Engineering and Physical Sciences Research Council, and the Scottish Higher Education Funding Council for funding through a Strategic Research Development Grant award. Solomon Saltiel and Kaloian Koynov thank the Bulgarian Ministry of Science and Education for support with Science Fund grant F-1201/2002.

REFERENCES

1. P.N. Prasad, in: *Introduction to Biophotonics* (Wiley & Sons, Hoboken, 2003) pp.203-254.
2. H. Schnitzler, U. Frohlich, T.K.W. Boley, A.E.M. Clemen, J. Mlynek, A. Peters, and S. Schiller, All-solid-state tunable continuous-wave ultraviolet source with high purity and frequency stability, *Applied Optics* **41**(33), 7000-7005 (2002).
3. R.S. Knox, Ultrashort processes and biology, *Journal of Photochemistry and Photobiology* **49,** 81-88 (1999).
4. W. Rudolph, P. Dorn, X. Liu, N. Vretenar, and R. Stock, Microscopy with femtosecond laser pulses: applications in engineering, physics and biomedicine, *Applied Surface Science* **208**, 327-332 (2003).
5. S.W. Hell, P.E. Hanninen, J. Salo, A. Kuusisto, E. Soini, T. Wilson, and J.B. Tan, Pulsed and cw confocal microscopy - a comparison of resolution and contrast, *Optics Communications* **113**(1-3), 144-152 (1994).
6. B. Agate, C.T.A. Brown, W. Sibbett, and K. Dholakia, Femtosecond optical tweezers for *in-situ* control of two-photon fluorescence, *Optics Express* **12(**13), 3011-3017 (2004).
7. P.J. Campagnola, M.D. Wei, A. Lewis, and L.M. Loew, High-resolution nonlinear optical imaging of live cells by second harmonic generation, *Biophysical Journal* **77**(6), 3341-3349 (1999).
8. E. Bordenave, E. Abraham, G. Jonusauskas, J. Oberle, and C. Rulliere, Longitudinal imaging in biological tissues with a single laser shot correlation system, *Optics Express* **10**(1), 35-40 (2002).
9. L. Zhu, P. Li, J.T. Sage., and P.M. Champion, Femtosecond dynamics of heme-proteins, *Journal of Luminescence* **60**(1), 503-506 (1994).

10. B. Agate, B. Stormont, A.J. Kemp, C.T.A. Brown, U. Keller, and W. Sibbett, Simplified cavity designs for efficient and compact femtosecond Cr:LiSAF lasers, *Optics Communications* **205**, 207-213 (2002).
11. B. Agate, E.U. Rafailov, W. Sibbett, S.M. Saltiel, K. Koynov, M. Tiihonen, S. Wang, F. Laurell, P. Battle, T. Fry, and E. Noonan, Portable ultrafast blue light sources designed with frequency doubling in KTP and $KNbO_3$, *IEEE Journal of Selected Topics in Quantum Electronics: Short Wavelength and EUV Lasers* (November/December 2004).
12. B. Agate, A. J. Kemp, C.T.A. Brown, and W. Sibbett, Efficient, high repetition-rate femtosecond blue source using a compact Cr:LiSAF laser, *Optics Express* **10**(16), 824-831 (2002).
13. B. Agate, E.U. Rafailov, W. Sibbett, S.M. Saltiel, P. Battle, T. Fry, and E. Noonan, Highly efficient blue-light generation from a compact diode-pumped femtosecond laser by use of a periodically poled KTP waveguide crystal, *Optics Letters* **28**(20), 1963-1965 (2003).
14. G. D. Boyd and D.A. Kleinman, Parametric interactions of focused Gaussian light beams, *Journal of Applied Physics* **39**, 3897-3641 (1968).
15. S. M. Saltiel, K. Koynov, B. Agate, and W. Sibbett, Second-harmonic generation with focused beams under conditions of large group-velocity mismatch, *Journal of the Optical Society of America B* **21**(3), 591-598 (2004).
16. A. M. Weiner, A. M. Kan'an, and D. E. Leaird, High-efficiency blue generation by frequency doubling of femtosecond pulses in a thick nonlinear crystal, *Optics Letters* **23**(18), 1441-1443 (1998).
17. D. Gunzun, Y. Li, and M. Xiao, Blue light generation in single-pass frequency doubling of femtosecond pulses in $KNbO_3$, *Optics Communications* **180**, 367-371 (2000).
18. Y.Q. Li, D. Guzun, G. Salamo, and M. Xiao, High-efficiency blue-light generation by frequency doubling of picosecond pulses in a thick $KNbO_3$ crystal, *Journal of the Optical Society of America B* **20**(6), 1285-1289 (2003).
19. S. Yu and A.M. Weiner, Phase-matching temperature shifts in blue generation by frequency doubling of femtosecond pulses in $KNbO_3$, *Journal of the Optical Society of America B* **16**(8), 1300-1304 (1999).
20. H. Wang and A.M. Weiner, Efficiency of short-pulse type-I second-harmonic generation with simultaneous spatial walk-off, temporal walk-off, and pump depletion, *IEEE Journal of Quantum Electronics* **39**(12), 1600-1618 (2003).
21. M. M. Fejer, G.A. Magel, D.H. Jundt, and R.L. Byer, Quasi-phase-matched second harmonic generation - tuning and tolerances, *IEEE Journal of Quantum Electronics* **28**, 2631-2654 (1992).
22. P. Loza-Alvarez, D.T. Reid, P. Faller, M. Ebrahimzadeh, W. Sibbett, H. Karlsson, and F. Laurell, Simultaneous femtosecond-pulse compression and second-harmonic generation in aperiodically poled $KTiOPO_4$, *Optics Letters* **24**(15), 1071-1073 (1999).
23. M.A. Arbore, O. Marco, and M.M. Fejer, Pulse compression during second-harmonic generation in aperiodic quasi-phase-matching gratings, *Optics Letters* **22**(12), 865-867 (1997).
24. R. DeSalvo, M. Sheik-Bahae, A.A. Said, D.J. Hagan, and E.W. Van Stryland, Z-scan measurements of the anisotropy of nonlinear refraction and absorption in crystals, *Optics Letters* **18**(3), 194 (1993).
25. A.D. Ludlow, H.M. Nelson, and S.D. Bergeson, Two-photon absorption in potassium niobate, *Journal of the Optical Society of America B* **18**(12), 1813-1820 (2001).
26. M. M. Fejer. Quasi-phasematched for frequency conversion and all optical signal processing (short course #1260) in *Conference on Lasers and Electro-Optics,* Baltimore (2001).
27. A. Yariv, *Quantum Electronics* (4ed, Wiley & Sons,1997)

28. M. Yamada, N. Nada, M. Saitoh, and K. Watanabe, First-order quasi-phase matched $LiNbO_3$ wave-guide periodically poled by applying an external-field for efficient blue second-harmonic generation, *Applied Physics Letters* **62**(5), 435-436 (1993).
29. S.N. Zhu, Y.Y. Zhu, Z.J. Yang, H.F. Wang, Z.Y. Zhang, J.F. Hong, C.Z. Ge, and N.B. Ming, Second-harmonic generation of blue-light in bulk periodically poled $LiTaO_3$, *Applied Physics Letters* **67**(3), 320-322 (1995).
30. H. Karlsson, F. Laurell, and L.K. Cheng, Periodic poling of $RbTiOPO_4$ for quasi-phase matched blue light generation, *Applied Physics Letters* **74**(11), 1519-1521 (1999).
31. H. Karlsson, F. Laurell, P. Henriksson, and G. Arvidsson, "Frequency doubling in periodically poled $RbTiOAsO_4$, *Electronics Letters* **32**, 556 (1996).
32. H. Karlsson and F. Laurell, Electric field poling of flux grown $KTiOPO_4$, *Applied Physics Letters* **71**(24), 3474-3476 (1997).
33. C. Canalias, J. Hirohashi, V. Pasiskevicius, and F. Laurell, Polarization switching characteristics of flux grown $KTiOPO_4$ and $RbTiOPO_4$ at room temperature, *Applied Physics Letters* (submitted), (2005).
34. K. Fradkin-Kashi and A. Arie, "Multiple-wavelength quasi-phase-matched nonlinear interactions, *IEEE Journal of Quantum Electronics* **35** 1649 (1999).
35. L.E. Myers, R.C. Eckardt, M.M. Fejer, R.L. Byer, and W.R. Bosenberg, "Multigrating quasi-phase-matched optical parametric oscillator in periodically poled $LiNbO_3$, *Optics Letters* **21**, 591 (1996).
36. K.A. Tillman, D.T. Reid, D. Artigas, J. Hellstrom, V. Pasiskevicius, and F. Laurell, Low-threshold, high-repetition-frequency femtosecond optical parametric oscillator based on chirped-pulse frequency conversion, Journal *of the Optical Society of America B* **20** 1309 (2003).
37. J.-M. Hopkins, G.J. Valentine, B. Agate, A. J. Kemp, U. Keller, and W. Sibbett, Highly compact and efficient femtosecond lasers, IEEE Journal of Quantum Electronics **38**(4), 360-368 (2002).
38. J.-M. Hopkins, G.J. Valentine, W. Sibbett, J.A. der Au, F. Morier-Genoud, U. Keller, and A. Valster, Efficient, low-noise, SESAM-based femtosecond Cr^{3+}:$LiSrAlF_6$ laser, *Optics Communications* **154**(1-3), 54-58 (1998).
39. W. Sibbett, B. Agate, C.T.A. Brown, A.A. Lagatsky, C.G. Leburn, B. Stormont, and E.U. Rafailov, Compact Femtosecond Oscillators (invited), in: *Ultrafast Optics IV*, edited by F. Krausz, (Springer Verlag 2004) pp. 3-21.
40. C.T.A. Brown, M.A. Cataluna, A.A. Lagatsky, E.U. Rafailov, B. Agate, C.G. Leburn, and W. Sibbett, Compact laser-diode-based femtosecond sources, *New Journal of Physics* **6**, 175 (2004).
41. G.J. Valentine, J.-M. Hopkins, P. Loza-Alvarez, G.T. Kennedy, W. Sibbett, D. Burns, and A. Valster, Ultralow-pump-threshold, femtosecond Cr^{3+}:$LiSrAlF_6$ laser pumped by a single narrow-stripe AlGaInP laser diode, *Optics Letters* **22**(21), 1639-1641 (1997).
42. A.A. Lagatsky, E.U. Rafailov, C.G. Leburn, C.T.A. Brown, N. Xiang, O.G. Okhotnikov, and W. Sibbett, Highly efficient femtosecond Yb:KYW laser pumped by a single narrow-stripe laser diode, *Electronics Letters* **39**(15), 1108-1110 (2003).
43. E.U. Rafailov, D.J.L. Birkin, W. Sibbett, P. Battle, T. Fry, and D. Mohatt, Efficient direct frequency conversion of a non-resonant injection-seeded laser diode using a periodically-poled KTP waveguide crystal, *Optics Letters* **26**(24), 1961-1962 (2001).
44. Y.S. Wang, V. Petrov, Y.J. Ding, Y. Zheng, J.B. Khurgin, and W.P. Risk, Ultrafast generation of blue light by efficient second-harmonic generation in periodically-poled bulk and waveguide potassium titanyl phosphate, *Applied Physics Letters* **73**(7), 873-875 (1998).

45. D.J.L.B. Birkin, E.U. Rafailov, G.S. Sokolovskii, W. Sibbett, G.W. Ross, P.G.R. Smith, and D.C. Hanna, 3.6mW blue light by direct frequency-doubling of a diode laser using an aperiodically-poled lithium niobate crystal, *Applied Physics Letters* **78**(21), 3172-3174 (2001).
46. D. Artigas and D.T. Reid, Efficient femtosecond optical parametric oscillators based on aperiodically poled nonlinear crystals, *Optics Letters* **27**(10), 851-853 (2002).
47. I.A. Begishev, M. Kalashnikov, V. Karpov, P. Nickles, H. Schonnagel, I.A. Kulagin, and T. Usmanov, Limitation of second-harmonic generation of femtosecond Ti:sapphire laser pulses, *Journal of the Optical Society of America B* **21**(2), 318-322 (2004).
48. I. Biaggio, P. Kerkoc, L.S. Wu, P. Gunter, and B. Zysset, Refractive-indexes of orthorhombic $KNbO_3$: Phase-matching configurations for nonlinear-optical interactions, *Journal of the Optical Society of America B* **9**(4), 507-517 (1992).
49. I. Shoji, T. Kondo, A. Kitamoto, M. Shirane, and R. Ito, Absolute scale of second-order nonlinear-optical coefficients, *Journal of the Optical Society of America B* **14**(9), 2268-2294 (1997).
50. G.G. Gurzadian, V.G. Dmitriev, and D.N. Nikogosyan, *Handbook of nonlinear optical crystals* (3ed), (Springer Verlag, New York, 1999).
51. L.E. Busse, L. Goldberg, M.R. Surette, and G. Mizell, Absorption Losses in MgO-doped and undoped potassium niobate, *Journal of Applied Physics* **75**(2), 1102-1110 (1994).